Surfactant free hydrothermal synthesis, electrical, optical and ferroelectric properties of $BaTiO_3$ nanoparticles

JASPREET KAUR, R.K. KOTNALA[a], KULDEEP CHAND VERMA[*]
Department of Physics, Eternal University, Baru Sahib, Sirmour (H.P.) 173101, India
[a]*National Physical Laboratory, New Delhi-110012, India*

Structural, microstructural, Raman spectroscopy, Photoluminescence, fourier transform infrared (FTIR) spectroscopy, dielectric, ac conductivity and ferroelectric properties of BaTiO3 (BT) nanoparticles were studied. BT nanoparticles were synthesized by a surfactant free hydrothermal method of processing temperature 200 ^{o}C/72h. The crystalline structure was investigated by X-ray diffraction and Raman spectroscopy show the tetragonal phase of BT. The average particle size and morphology were examined by transmission/scanning electron microscopy. Photoluminescence shows the green emission result in recombination of a photo generated hole with a singly ionized charged state. FTIR measurement shows the existence of Ba-Ti-O bond. Frequency dependent dielectric properties, i.e., relative dielectric permittivity and dielectric loss were studied in the frequency range 1 kHz - 10 MHz. The dielectric behavior is explained by the interface polarization, decreasing trend of the dielectric permittivity with increasing frequency by the Koops model, dispersion by Maxwell-Wagner type and is constant up to higher frequency region due to nano size effect. The *ac* conductivity with varying frequency at room temperature increases with increasing frequency. Polarization dependent electric field measurement is used to represent ferroelectric behavior of BT nanoparticles.

(Received January 30, 2012; accepted April 11, 2012)

Keywords: $BaTiO_3$, Hydrothermal synthesis, TEM/SEM, Raman Spectra, Electrical and ferroelectric properties, Photoluminescence

1. Introduction

Perovskite metal oxides such as $BaTiO_3$, $PbTiO_3$, $SrTiO_3$ etc. [1-5] have been widely investigated due to their outstanding dielectric and ferroelectric properties. These ferroelectric materials exhibit two features, namely, the existence of spontaneous polarization and the possibility to reorient the polarization by an external electric field. As a result these properties make ferroelectrics very attractive for non-volatile ferroelectric memories, thin film capacitors, piezoelectric sensors, actuators, pyroelectric detectors, as well as domain switching which is the predominant source of the non-linear dielectric behavior [3,4]. Recent advanced technology in the synthesis and fabrication of ferroelectrics has attributed in the down-scaling of feature sizes of ferroelectric based electronic devices into nanoscale dimensions, at which there is a significant deviation of the properties from their bulk form. Ferroelectric $BaTiO_3$ (BT) is a key material used as dielectric in ceramic capacitors, integral capacitors in printed circuit boards owing to its high dielectric constant not only in bulk crystals but also for nanocrystals. Pure BT is an excellent insulator with large energy gap ~ 3.05 eV at room temperature. In BT, the cations and anions get separated, which results in spontaneous polarization and a high dielectric constant that are strongly dependent on the particle size. The delicate balance between long range coulomb interaction and short range covalent interaction results in atomic off-centre displacements, which cause ferroelectricity of BT [5]. Also, BT at room temperature exhibits tetragonal symmetry with spontaneous polarization along the *c*-axis which occurs due to the non-centrosymmetric displacement of Ti^{4+} and O^{2-} ions relative to Ba^{2+}.

Along with ferroelectric properties, BT also exhibits optical properties such as photoluminescence (PL) that provides valuable information on the quality and purity of material, along with the visible transition emission. In PL, the photon excitation is followed by emission process in which the electrons eventually fall back down to the valence band; the energy it loses is converted back in luminescent photon. Various chemical methods such as sol-gel, co-precipitation, chemical combustion, hydrothermal process etc. [6-8] are used to fabricate BT nanoparticles with high purity and uniform size distribution. Among them hydrothermal method is of considerable interest because of its promising advantages such as low particle agglomeration, high-purity and single-phase oxides can be obtained in a single step from inexpensive and easily accessible precursors. Also in hydrothermal, a simple autoclave is used which has mild reaction temperature not only reduce the energy cost but also enhance the reactivity of the products [9]. Dynamic interactions between Ti^{4+}, Ba^{2+}, and the surrounding solution lead to the crystallization of BT during hydrothermal treatment. There are two main formation mechanisms that describe the hydrothermal synthesis. One is dissolution and precipitation, in which Ba^{2+} aqueous species react with hydrolyzed Ti species to form nuclei. And second is in-situ transformation, which involves diffusion of Ba^{2+} into the undissolved TiO_2 oxide, resulting

in an outside layer of BT with an unreacted TiO_2 core [10, 11]. With low temperature synthesis, a monitor crystallization behavior allows easier sampling throughout the reaction and makes it possible to observe microstructural evidence for the reaction mechanism [10].

In this work, we present the structural, microstructural, photoluminescence, Raman spectra, fourier transform infrared (FTIR) spectroscopy, ferroelectric and electrical properties of hydrothermally synthesized BT nanoparticles.

2. Experimental

BT nanoparticles were fabricated via hydrothermal process at 200 ^{o}C using barium acetate, tetra-n-butyl orthotitanate and ferric chloride (all of analytical grade) as the starting materials, NaOH served as an alkaline mineraliser. Firstly, known amount of barium acetate was dissolved in distilled water and tetra-n-butyl orthotitanate was dissolved in ethanol to form a uniform solution by stirring, respectively. Subsequently, the latter solution was slowly dropped into the barium acetate solution under constant-rate stirring, and the pH value of the mixed solution was adjusted to 13 by adding NaOH. The final reaction mixture was violently stirred and then poured into a Teflon vessel until 80% of its total volume, and then the vessel was placed in a stainless steel tank to perform the hydrothermal treatment at 200 °C for 72h. After the autoclave was cooled down to room temperature naturally, the obtained products were washed several times with distilled water and ethanol, respectively, and dried at 80 °C for 8h. Finally, a powder form BT was obtained. The crystalline structure was analysed by X-ray diffraction (XRD) using X'Pert PRO PANalytical system. The microstructure was analyzed by transmission electron microscopy (TEM) using HITACHI H-7500 and scanning electron microscopy (SEM) using JEOL JSM 6100. PL and Raman spectrum of the specimen was recorded at room temperature on Renishaw UK which consists of Ar ion laser with 514.5 nm wavelength and 50 mW power. The FTIR was recorded on Perkin Elmer spectrum 400 FTIR/FT-FIR spectrometer. Polarization was measured using Radiant Technologies ferroelectric test system. The electrical measurements were performed at room temperature using impedance analyzer (4200 semiconductor character unit, CVU module).

3. Results and discussion

Fig. 1 shows the XRD pattern of the prepared BT nanoparticles with hydrothermal condition of 200 ^{O}C/72h. It shows sharp, well-defined diffraction peaks, indicating good crystallinity. The observation of the peaks (001) and (100) confirms the tetragonal structure of BT which is further confirmed by Raman spectra in Fig. 4. In addition, analysis of the XRD data indicated that the lattice parameters are a (Å) = 3.996 and c(Å) = 4.041. The tetragonal distortion (c/a) is 1.0112. So all the diffraction peaks can be assigned to tetragonal BT phase. No other impurity was observed. The average particle size (x) was calculated by using Debye-Scherer relation

$$x = \frac{0.9\,\lambda}{\beta\, cos\theta} \quad (1)$$

where λ is the wavelength and θ is the angle of diffraction. The average particle size is calculated to be 10 nm.

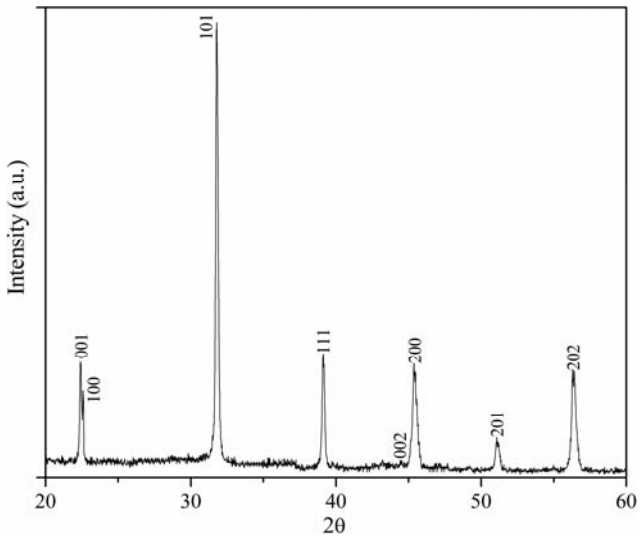

Fig. 1 X-ray diffraction pattern of BT nanoparticles prepared at 200 ^{o}C/72h.

The BT morphology and structure have been studied using TEM and SEM as shown in Figs 2 & 3, respectively. Fig. 2 shows TEM image which reveals that the particle is nearly spherical and has an average size of 11 nm. The SAED pattern [inset of Fig.2] reveals the single-crystalline nature of BT nanoparticles without any sheath of amorphous phase. According to the SEM images [seen from Fig. 3], the average particle size is 12 nm which is in close agreement with that confirmed by XRD and TEM results.

Raman spectroscopy is highly sensitive spectroscopic technique to explain the local and dynamic symmetries of atoms in the materials. Figure 4 shows the Raman spectra of BT nanoparticles. Raman shift peaks located at around 248.33, 305.86, 516.39 and 715.10 cm^{-1} of BT are closely in agree with tetragonal BT nanoparticles reported in the literature [12]. The broad peaks at 248.33 cm^{-1} is assigned to the fundamental TO mode of A_1 symmetry i.e. [A_1(TO)] and the peak at 305.86 cm^{-1} is assigned to [B_1, E(TO + LO)] mode indicating the asymmetry of TiO_6 octahedra within the BT structure [12, 13]. The peak around 715.10cm^{-1} [A_1(LO), E(LO)] is related to the highest frequency longitudinal optical mode (LO) with A_1 symmetry [4, 14]. Peak at around 186.27cm^{-1} explains the presence of TiO_2 anatase phase usually detected in low crystalline structures which may also be seen in XRD pattern by small distortion. The presence of asymmetry in

the peak at 516.39 cm^{-1} [A_1(TO), E(TO)] suggests the existence of coupling of TO modes associated with the tetragonal phase. These results agree well with the XRD results.

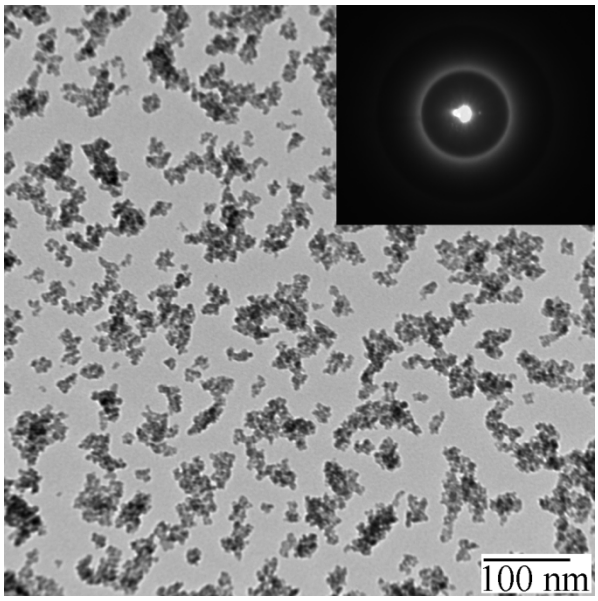

Fig. 2 Transmission electron microscopy for BT nanoparticles.

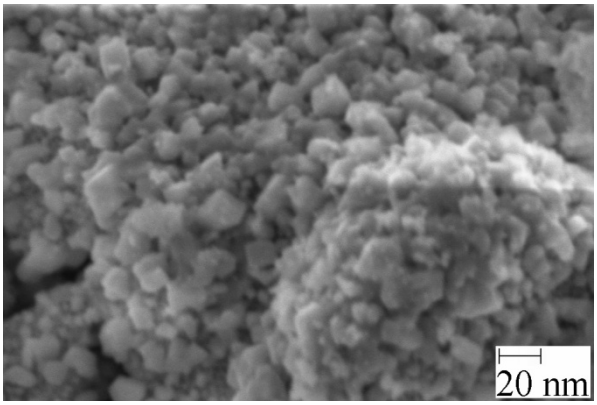

Fig. 3 Scanning electron microscopy BT nanoparticles.

The efficiency of trapping, transfer and separation of charge carriers, and investigation of lifetime in semiconductor, were revealed by the PL emission spectra that results from the recombination of free charge carriers [15]. Figure 5 shows PL spectra of BT nanoparticles excited with 514.5 nm laser source at room temperature. Point defects such as oxygen vacancies and complexes involving barium interstitials are known to contribute to deep level emission in the visible spectrum.The intense emission peaks were observed between 520 to 550 nm, i.e., the emission region of green light which is most likely due to self-activated defect centers formed inside the lattice. A broad band was also observed centered at around 623 nm and represents the yellow light emission. The inset of Fig. 5 shows the PL spectra in the range 520 to 550 nm. All the peaks observed in this range i.e., at λ = 522.70, 528.59, 534.11, and 544.16 nm come in the region of green light emission. The intense peak at λ = 522.70 nm relates to intra-band transitions, i.e., between levels created by defects within the band gap, caused by the oxygen vacancies. The peak at 528.59 nm can be attributed to singly ionized oxygen vacancy. The recombination via surface localized states is explained by a weak emission peak at λ = 544.18 nm. The green emission is the result of recombination of a photo generated hole with a singly ionized charged state. The intensity of PL emission depends mainly on the interaction between these complex clusters and the excitation wavelength.

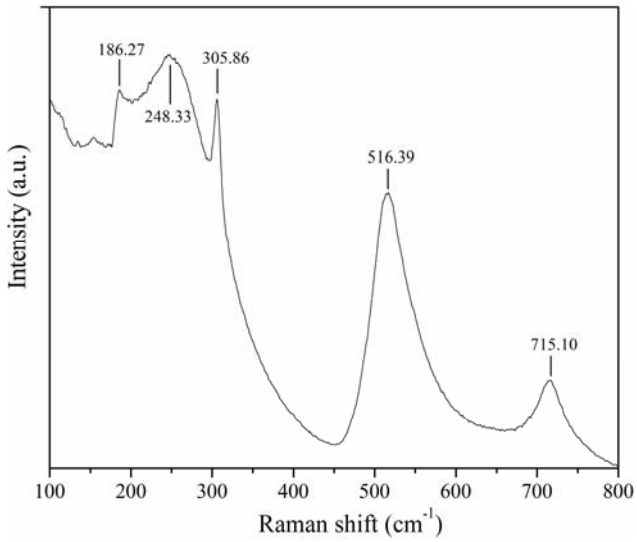

Fig. 4 Raman spectra of BT nanoparticles

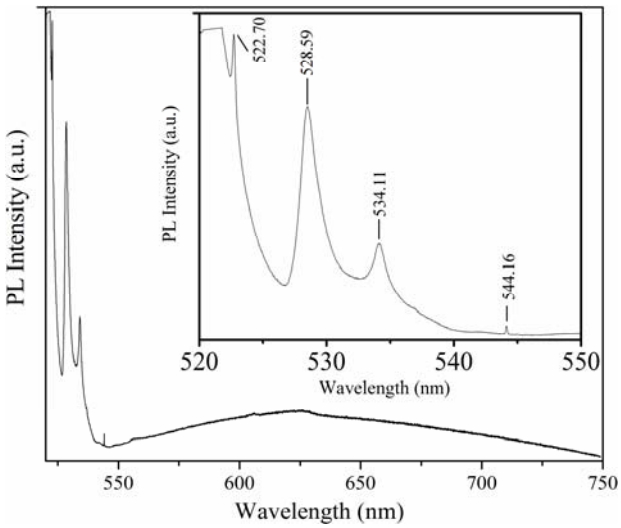

Fig. 5 Photoluminescence spectra of BT nanoparticles

The formation of BT was further evaluated by FTIR measurement, as shown in Fig. 6. The FTIR studies of BT

nanoparticles shows small absorption bands at around 3424.25, 2344.75, 1607.46, and 548.73 cm^{-1}. A band centred at 3424.25 cm^{-1} corresponds to lattice water absorbed (antisymmetric and symmetric OH stretching). The small band present at 2344.75 cm^{-1} in the spectrum is due to adsorbed CO_2 corresponding to C-H stretching vibrations [16] and at 1607.46 cm^{-1} is due to the organic groups bonded to titanium representing the –OH stretching mode. The band at 548.73 cm^{-1} corresponds to the Ba-Ti-O stretching vibration. FTIR spectrum shows similar an -OH stretching modes at ~3400 cm^{-1} and 1600 cm^{-1} observed by Joshi *et al.* [4].

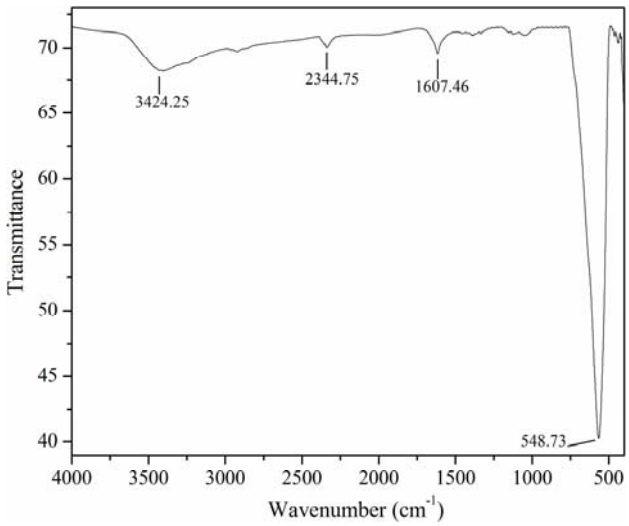

Fig. 6 Fourier transform infrared spectroscopy of BT nanoparticles

Fig. 7 shows the frequency dependent relative permittivity (ε) and dielectric loss (*tanδ*) of BT nanoparticles measured at room temperature. At 1 MHz, BT shows dielectric constant 130 with *tanδ* 0.010. The *ε* and *tanδ* decreases rapidly with increasing frequency and reaches a constant value at higher frequency. This can be explained on the basis of space charge polarization due to inhomogeneous dielectric structure. It is also based on the fact that beyond a certain frequency of electric field the electron exchange does not follow the alternating field. However, it shows dispersion in *ε* and *tanδ* at lower frequency region. This result suggests that it might be due to Maxwell-Wagner interfacial polarization [17] which is also in agreement with Koops theory [8]. Accordingly, a dielectric medium is assumed to be made of well conducting grains which are separated by resistive (poor conducting) grain boundaries. The slight variation in the dielectric constant in the middle frequency region is explained on the basis of Stoner-Wohlfarth model [19] of nanoparticles.

Fig. 8 shows the frequency dependent *ac* conductivity measured at room temperature. Electrical conductivity effect gives rise to higher values of dielectric constant, which decreases with increasing frequency. It can be observed that *ac* conductivity (σ_{ac}) increases with increasing frequency. The relation between σ_{ac} and ε is given by

$$\sigma_{ac} = \varepsilon\omega\varepsilon_0 \quad (2)$$

where σ_{ac} is the *ac* conductivity, $\omega = f \times 2\pi$ (f is the measuring frequency) and ε_0 is the free space permittivity. This increase of *ac* conductivity with frequency is attributed to the trapped bound carriers in the sample resembling hopping type conduction. The increase in conductivity can also be explained by two other explanations. One is the enhanced dielectric relaxation of the polarization of the BT nanoparticles in a high frequency region and second is electric energy associated with high *ac* frequency which encourages the electric charge to jump between the nanosize particles [20]. The value of *ac* conductivity is observed to be the order of 10^{-9} $(\Omega cm)^{-1}$.

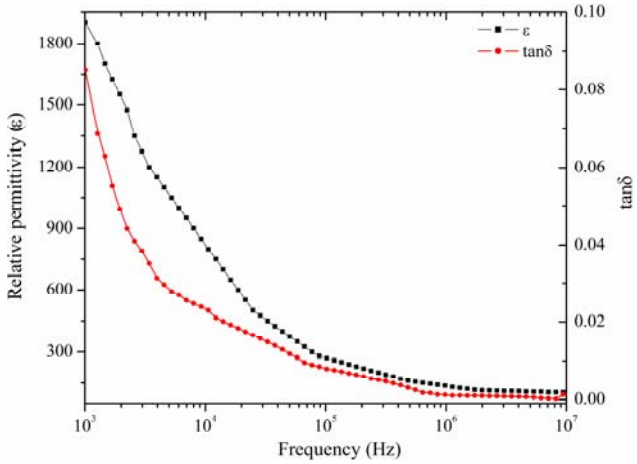

Fig.7. Frequency dependent relative permittivity measured at room temperature.

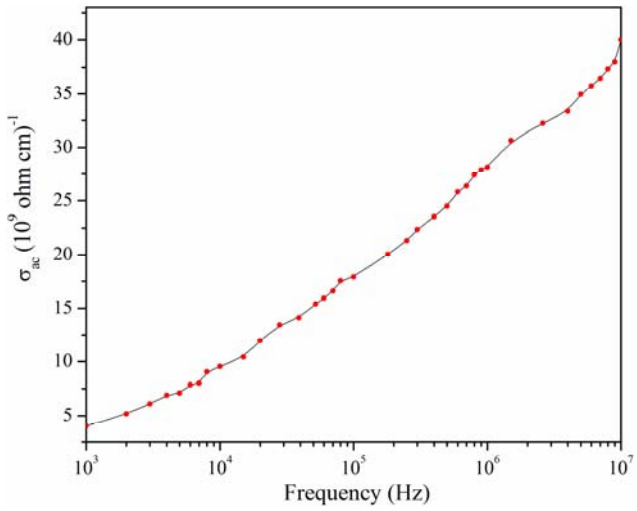

Fig. 8 Frequency dependent ac conductivity at room temperature.

Fig. 9 shows ferroelectric hysteresis loop by measuring polarization versus applied electric field (*P-E*) at room temperature. It is observed that BT exhibits saturated hysteresis loop with spontaneous polarization P_s~ 27.43 μC/cm^2, remanent polarization P_r~ 18.32 μC/cm^2, and coercive field E_c~ 23.57 kV/cm. Compared with the result in our previous work of BT [21] prepared by sol-gel technique, the present BT nanoparticles has polarization value decreases because of very small nanograins have higher value of *dc* resistivity.

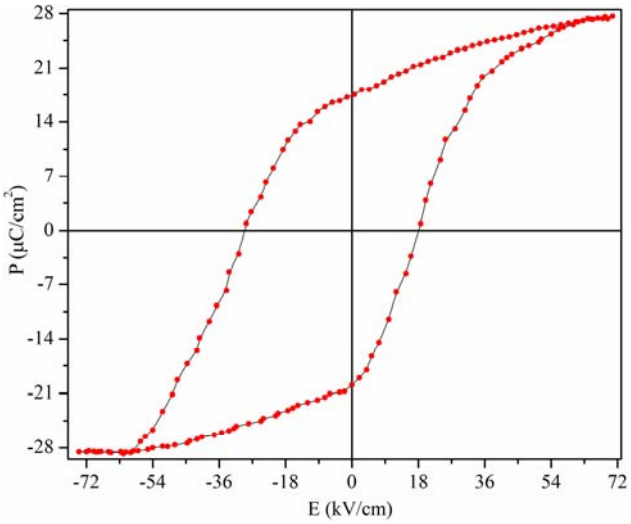

Fig. 9 Polarization versus applied electric field (P-E) hysteresis of BT nanoparticles.

4. Conclusion

We have synthesized BT nanoparticles through hydrothermal method with reaction temperature 200 °C/72 hrs. XRD pattern shows tetragonal structure of BT. The average particles size measured by TEM 11 nm and by SEM 12 nm are in close agreement with that calculated by XRD peaks. The peaks in the Raman spectra also correspond to the tetragonal symmetry of BT. The FTIR spectra show the existence of metal-oxygen bond (Ba-Ti-O). The PL spectra of the as-synthesized BT nanoparticles show the optical nature. At 1 MHz, BT nanoparticles shows the value of dielectric constant 130 with *tanδ* 0.010 and dispersion less dielectric response at higher frequencies. The *ac* conductivity with varying frequency at room temperature increases with increasing frequency and is of the order of $(10^9\ \Omega cm)^{-1}$. The value of spontaneous polarization P_s ~ 27.43 μC/cm^2, remanent polarization P_r ~ 18.32 μC/cm^2, and coercive field E_c ~ 23.57 kV/cm are observed.

References

[1] J.F. Scott, F.D. Morrison and M. Miyake, J. Am. Ceram. Soc. **88**, 1691 (2005).
[2] K.C. Verma, M. Singh, N. Thakur, N.S. Negi, International J. Modern Phys. B **24**(23), 4547 (2010)
[3] M. Dawber, K.M. Rabe, J.F. Scott, Rev. Mod. Phys.**77**, 1083 (2005).
[4] I. Chilibon, J.M. Mendes, R. Igreja, C.J. Dias, J. Optoelectron. Adv. Mater. **7**(5), 2727 (2005).
[5] U.A. Joshi, S. Yoon, S. Baik and J.S. Lee, J. Phys. Chem. B **110**, 12249 (2006).
[6] K.C. Verma, R.K. Kotnala, N. Thakur, V.S. Rangra, N.S. Negi, J. Appl. Phy. **104**, 093908 (2008).
[7] T. Yan, X-L. Liu, N.R. Wang and J.F. Chen, J. Cryst. Growth **281**, 669 (2005).
[8] M. Cernea, J. Optoelectron. Adv. Mater. **11**(8), 1191 (2009).
[9] S.K Tripathy, T. Sahoo, M. Mahapatra, S. Anand, R.P. Das, Mater. Lett. **59**, 3543 (2005).
[10] W. Hertl, J.Am Ceram. Soc. **71**(10), 879 (1988).
[11] I. Maclaren and C.B. Ponton, J. Eur. Ceram. Soc. **20**, 1267 (2000).
[12] H. Hayashi, T. Noguchi, N.M. Islam, Y. Hakuta, Y. Imai, N. Ueno, J. Cryst. Growth **312**, 3613 (2010).
[13] Y. Shiratori, C. Pithan, J. Dornseiffer, R. Waser, J. Raman. Spectrosc. **38**, 1288 (2007).
[14] X. Zhu, J. Wang, Z. Zhang, J. Zhu, S. Zhou, Z. Liu N. Ming, J. Am. Ceram. Soc. **91(8)**, 2683 (2008).
[15] J.G. Yu, L. Yue, S.W. Liu, B.B. Huang, X.Y. Zhang, J. Colloid Interface Sci. **58**, 334 (2009).
[16] M. Cernea, J. Optoelectron. Adv. Mater. **7**(6), 3015 (2005).
[17] R.P. Mahajan, K.K. Patankar, M.B. Kothale, S.A. PatilBull. Mater. Sci. **23(4)**, 273 (2000).
[18] C.G. Koops, Phys. Rev. **83**, 121 (1951).
[19] C. Tannous, J. Gieraltowski, Eur. J. Phy. **29**, 475 (2008).
[20] A.Tataroglu, S. Altindal, M.M. Bulbul, Microelectron. Eng. **81**, 140 (2008).
[21] J. Kaur, R.K. Kotnala, K.C. Verma, Matter. Lett. **65**, 3160 (2011).

Corresponding author:* kuldeep0309@yahoo.co.in